Myosin Va maneuvers through actin intersections and diffuses along microtubules

M. Yusuf Ali*†, Elena B. Krementsova*, Guy G. Kennedy*, Rachel Mahaffy‡, Thomas D. Pollard‡§, Kathleen M. Trybus*, and David M. Warshaw*

*Department of Molecular Physiology and Biophysics, University of Vermont, Burlington, VT 05405; and ‡Department of Molecular, Cellular, and Developmental Biology, Yale University, New Haven, CT 06520

Contributed by Thomas D. Pollard, December 26, 2006 (sent for review November 6, 2006)

Certain types of intracellular organelle transport to the cell periphery are thought to involve long-range movement on microtubules by kinesin with subsequent handoff to vertebrate myosin Va (myoVa) for local delivery on actin tracks. This process may involve direct interactions between these two processive motors. Here we demonstrate using single molecule *in vitro* techniques that myoVa is flexible enough to effectively maneuver its way through actin filament intersections and Arp2/3 branches. In addition, myoVa surprisingly undergoes a one-dimensional diffusive search along microtubules, which may allow it to scan efficiently for kinesin and/or its cargo. These features of myoVa may help ensure efficient cargo delivery from the cell center to the periphery.

cytoskeleton | molecular motor | motility | processivity

Coordinated organelle transport along certain secretory pathways starts with kinesin-powered movement on microtubules and finishes with vertebrate myosin Va (myoVa)-based motility on actin (1–4). This trip requires that both motors be present when a microtubule–actin intersection is encountered, but how these two motors find one another or the cargo they share is still unknown. Another challenge is to understand how cargo is delivered to its destination by way of the complex cytoskeletal network. Vertebrate myoVa is a processive motor that can travel long distances along its actin track (5). However, the cytoskeletal intersections that myoVa must encounter along its journey may present a physical barrier to forward motion or an alternate path to its final destination.

To investigate this issue from myoVa's point of view, we observed single myoVa molecules labeled with highly photostable quantum dots (Qdots) in an objective-type total internal reflectance microscope (6) as they maneuvered through a model of cytoskeletal intersections created on a microscope coverslip coated with either actin filaments (Fig. 1*A*) or actin filaments and microtubules (Fig. 1*B*). In this model system, actin–actin intersections could inhibit or alter myoVa's direction of travel while actin-microtubule intersections should act as a hurdle to myoVa's processive movement. Given myoVa's ability to take 72-nm steps as it walks processively along actin filaments in a hand-over-hand fashion (6–9) and its inherent flexibility (10, 11), we have observed that myoVa can easily maneuver past actin filament intersections. In contrast, when encountering a microtubule, myoVa cannot step over this physical barrier, but surprisingly can step onto the microtubule and begin a one-dimensional diffusive search. Thus, myoVa has evolved to handle the challenges of the cytoskeletal network and through its interaction with the microtubule can effectively scan for its transport partner, kinesin, and/or its cargo.

Results and Discussion

MyoVa Dynamics at Actin Filament Intersections. To determine what happens when myoVa encounters an overlapping actin filament, we adhered Alexa Fluor 660 phalloidin-labeled actin filaments to the coverslip, followed by TRITC-phalloidin-labeled actin filaments (Fig. 1*A*). Thus, the TRITC filaments all lay over the Alexa Fluor filaments, providing a hurdle to myoVa.

We observed 171 individual myoVa molecules approaching an actin filament intersection and found that they took three options: 15% stepped over the intersecting actin; 37% terminated their movement at the intersection; and the remaining 48% turned left or right with equal probability [Fig. 2 and supporting information (SI) Movies 1–3]. A fourth option was that the intersecting actin filament created an effective, 7-nm-high "underpass" through which myoVa could travel. However, given myoVa's size and the ≈15-nm diameter of the attached Qdot, it is unlikely that myoVa could squeeze through this gap. When turning at an intersection, the direction taken was determined by the polarity of the intersecting TRITC-actin filament, so the myoVa stepping mechanism has no apparent bias that favors turning one direction over the other. Because myoVa can cross over an actin filament, the leading head must lift off its actin track by at least the 7-nm diameter of the intersecting actin filament. MyoVa must also possess considerable flexibility (10), because it turned at intersections through angles between 10° and 150°. This flexibility might exist at the junction between the coiled-coil region and the individual necks (11). The flexibility allows the lead head to sample actin monomers within a target zone defined by its potential 50- to 95-nm stepping range (6, 8) while its trailing head is attached to the lower filament (Fig. 3*B*). Although some monomers may not be available for myosin binding due to the geometry and the mode of actin filament attachment to the coverslip, a simple structural model (Fig. 3*B*) suggests that ≈40 available actin monomers exist within the target zone; 80% providing potential binding sites for turning, whereas only 20% may allow the lead head to step over the intersecting actin. This calculated 4:1 ratio of turning at-to-stepping over an intersecting actin is remarkably similar to the observed 48% turning and 15% crossover frequency. The 48% turning probability may be the basis for the 50% switching probability between actin filaments that has been predicted for melanosomes being transported by a single myoVa (12).

An intersecting actin filament also represents a physical barrier, because the probability of termination at an intersection (37%) is 3-fold greater than predicted based on previous myoVa processivity studies with single linear actin tracks (13, 14). To address this with high spatial resolution (Fig. 3*A*), the stepping

Author contributions: M.Y.A., G.G.K., T.D.P., K.M.T., and D.M.W. designed research; M.Y.A., E.B.K., and G.G.K. performed research; E.B.K., R.M., T.D.P., and K.M.T. contributed new reagents/analytic tools; M.Y.A., G.G.K., K.M.T., and D.M.W. analyzed data; and M.Y.A., T.D.P., K.M.T., and D.M.W. wrote the paper.

The authors declare no conflict of interest.

Abbreviations: myoVA, myosin VA; Qdot, quantum dot.

†On leave from: Department of Physics, Shah Jalal University of Science and Technology, Sylhet-3114, Bangladesh.

§To whom correspondence should be addressed. E-mail: thomas.pollard@yale.edu.

This article contains supporting information online at www.pnas.org/cgi/content/full/0611471104/DC1.

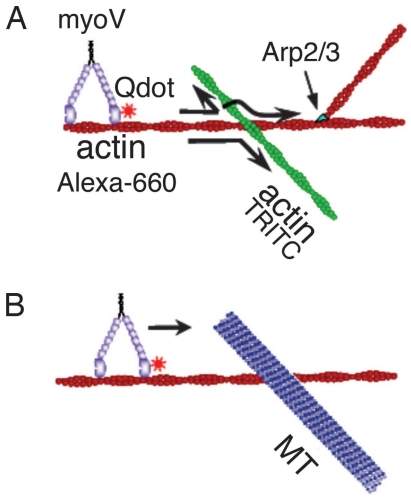

Fig. 1. Illustration of *in vitro* cytoskeletal intersection model and experimental design. (*A*) To model myoVa's ability to maneuver through the actin cytoskeleton, actin intersections were created on a coverslip by first attaching Alexa Fluor 660 (red) actin followed by TRITC-actin filaments (green). In addition, branched filaments were created by using Arp2/3 (see *Materials and Methods*). (*B*) Microtubular-actin intersections were created on a coverslip by first attaching Alexa Fluor 660 actin followed by rhodamine-labeled microtubules (see *Materials and Methods*).

rate was slowed to 0.3 s^{-1} using 500 nM ATP and then the distance between the final position of the myoVa molecule and the actin filament intersection was measured, as well as the lifetime of the last step before termination. Based on the lead head's stepping range (see above), termination distances >100 nm from the intersection must be a spontaneous termination (Fig. 3*C*). Closer inspection of the data within 100 nm of the intersection suggests that these data are well fit by a single Gaussian centered at 51 ± 3 nm (Fig. 3*C*). Because ≈72-nm steps were routinely observed (Fig. 3*A*), the myoVa molecule must be labeled with a Qdot on only one of its heads, but without knowing which head is labeled, 51 nm most likely represents the

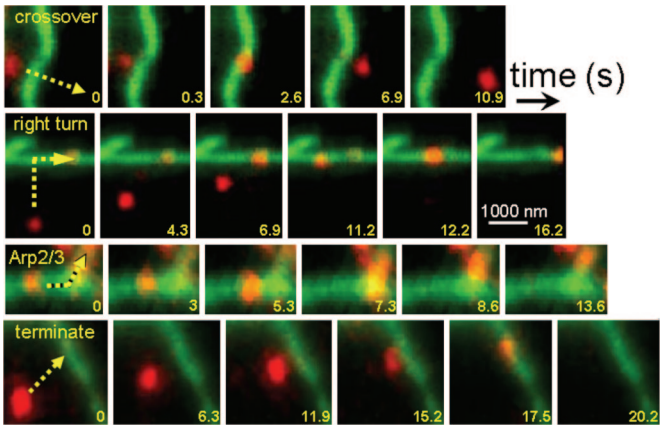

Fig. 2. Sequential images of Qdot-labeled myoVa encountering various forms of actin filament intersections. A single myoVa motor (red dot) travels along an Alexa Fluor 660 phalloidin-labeled actin filament (not visible due to rapid photobleaching) in the sequences labeled ''crossover,'' ''right turn,'' and ''terminate'' before encountering a TRITC phalloidin-labeled actin filament (green). The TRITC actin filaments are draped over the Alexa Fluor 660 actin filaments based on the order of actin filament addition to the flow cell. The time sequence is shown in the lower right corner. In the sequence labeled ''Arp2/3,'' a myoVa motor travels along a TRITC actin filament (green) before encountering an Arp2/3 branch, which it takes up to the top of the image.

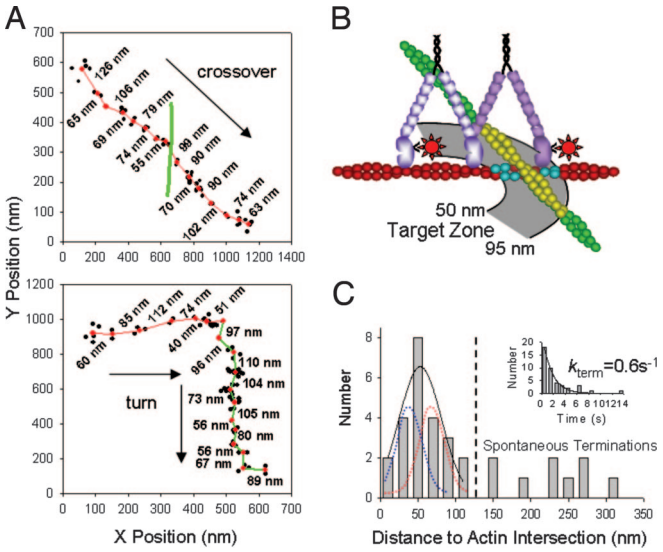

Fig. 3. High spatial resolution analysis of myoVa encountering actin filament intersections. (*A*) MyoVa X, Y-positional information are shown as it travels in 500 nM ATP along an Alexa Fluor 660 actin filament (red line) and either crosses over or turns onto a TRITC actin filament (green line). The myoVa position (black circles) was determined by using FIONA every 0.33 s and, when paused at each step, multiple data points were averaged to give a final position (red circles). The distance between these final positions are provided. For the crossover example, the myoVa takes a 99-nm step to make it over the TRITC actin filament while taking 83 ± 19-nm steps during its run. For the turning example, the myoVa motor took a 51-nm step to switch to the intersecting filament while taking 80 ± 22-nm steps over its entire run. (*B*) Simple model explaining turning versus crossover frequency. MyoVa (light purple) at final position on Alexa Fluor 660 actin (red) before encountering a TRITC actin intersection (green). The Qdot-labeled trailing head (red star), when undergoing its step to its new position as the leading head (dark purple), undergoes a diffusional search that samples the available actin monomers (30 yellow and 7 blue monomers) within a 50- to 95-nm target zone (gray arc), determined by the range of distances normally observed between heads while paused on actin. The ratio of yellow or blue monomers to the 37 total monomers within the target zone gives an estimate of the probability for turning versus crossing over. (*C*) Histogram of the final myoVa distance to an actin intersection that resulted in run termination. Distances >100 nm were considered spontaneous terminations. Distances <100 nm were well fit by a Gaussian (51 ± 3 nm), which most likely represents the myosin's center of mass (see text). With only one head Qdot labeled and with a probability of labeling being equal for the two heads, it may be possible with sufficient data to resolve two Guassians (hypothetical blue and red dotted lines) that are 36 nm apart representing each of the heads. (*Inset*) A histogram of the lifetime of the last step before termination, resulting in an effective termination rate of 0.6 s^{-1}.

myoVa's center of mass (see Fig. 3*C*). Knowing that, while paused on actin, the two heads are separated by 36 nm (6, 15), this would place the trailing head at 69 nm [i.e., 51 nm + (36/2) nm] from the intersection. Therefore, the next ≈72-nm step by the trailing head would have it land right on the intersection, but in this case being unable to find an appropriate actin monomer, it terminates its run at a rate of 0.6 s^{-1} (Fig. 3*C Inset*) similar to the 1 s^{-1} termination rate previously reported (13, 16).

We also observed myoVa navigating past actin filament branches formed by the Arp2/3 complex (17, 18). Given myoVa's apparently large turning radius and with the Arp2/3 complex being only slightly larger than two actin subunits, it is not surprising that myoVa can travel down a branch (Fig. 2). Analysis of 76 individual myoVa molecules showed that 62% continued along the mother filament and 20% switched to the Arp2/3 branch with equal probability for branches originating on the right or left side of the mother filament. The remaining 18% dissociated near a branch, either as a result of a spontaneous termination (13) or because the leading head attempted to step

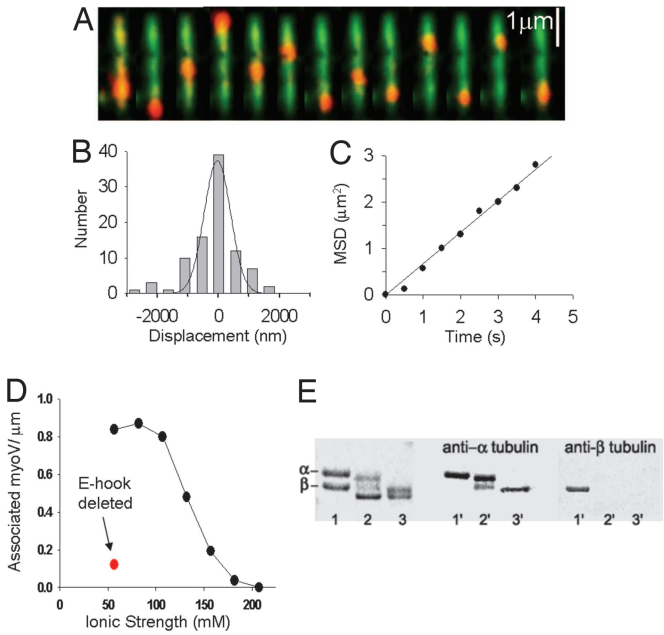

Fig. 4. One dimensional diffusive search of myoVa on microtubules. (*A*) Images of Qdot-labeled myoVa (red) diffusing on TRITC-labeled microtubule. The sequence of images was obtained at the following times in seconds starting from the left: 0, 6, 9.6, 14.6, 22.6, 27.9, 37.2, 40.2, 43.5, 57.5, 69.5, 82.2, 86.5. (*B*) Images as in *A* were analyzed to determine the displacement between successive image frames (three frames per s) and then plotted as a displacement histogram. A single Gaussian was fit to the data using the equation: $y = a \exp[-0.5((x - x_o)/b)^2]$, with the following parameters: $a = 37.39$, $b = 431.53$ nm, and $x_o = -34.7$ nm. From these data, the variance $= 2Dt$, where D is the diffusion coefficient and t is the time interval between images, resulting in $D = 0.28$ μm^2/s. (*C*) The mean square displacement (MSD) is plotted versus time, with the slope providing an estimate of D, as follows: $D = \langle \Delta x^2 \rangle / 2t$, where Δx is the change in distance measured from the starting point of the record during time interval t. For this example, $D = 0.33$ μm^2/s. (*D*) The number of myoVa per μm of microtubule length that were associated and diffusing on the microtubule was determined as a function of ionic strength by varying [KCl]. The [myoVa] in solution was 1.25 nM. Upon subtilisin treatment of tubulin to remove the charged E-hook, the number of associated myoVa/μm microtubule (red filled circle) decreased significantly at 25 mM KCl (57 mM ionic strength equivalent). (*E*) Cleavage of the C-terminal E-hook from microtubules. (*Left*) SDS/8% PAGE gel of undigested microtubules (lane 1), and after digestion with increasing concentration of subtilisin (lanes 2,3; see *Methods*). (*Right*) Immunoblots of these three lanes with anti-α or anti-β tubulin antibodies. Cleavage of the E-hook of β-tubulin results in loss of epitope reactivity.

onto the Arp2/3 complex but was unable to bind. Thus, the Arp2/3 complex and its associated branch provide myoVa an alternate route to its destination.

MyoVa Diffuses on Microtubules. Of the 58 myoVa molecules that approached a 25 nm diameter microtubule lying across the actin track (Fig. 1*B*), the majority were unable to step over. Surprisingly, four stepped onto the microtubule and diffused randomly back and forth (SI Movie 4). Many additional myoVa molecules associated directly with microtubules (≈1 myoVa per μm of microtubule) even in the absence of actin filaments on the coverslip (Fig. 4*A*, SI Fig. 6, and SI Movie 5). This motion of myoVa on microtubules does not require ATP. Control experiments showed that neither Qdots alone nor Qdot-labeled biotin-BSA associate with microtubules (data not shown), suggesting a myoVa-specific interaction with the microtubule.

The distribution of myoVa displacements on microtubules between successive images is a Gaussian centered at zero displacement (Fig. 4*B*), as expected for a one-dimensional diffusive search (19). The slope of the mean square displacement versus time (Fig. 4*C*) provides an estimate of the diffusion coefficient of Qdot-labeled myoVa of 0.26 ± 0.06 (SEM) μm^2/s, $n = 31$. This value is similar to the diffusion coefficient associated with the one-dimensional diffusive search of the depolymerizing kinesin, MCAK (20). Therefore, myoVa can rapidly (average maximum speed = 3.1 ± 0.4 μm/s, $n = 31$) scan distances as large as 1.8 ± 0.1 μm ($n = 31$) with an interaction lifetime of 47 ± 5 s ($n = 70$) before dissociating from the microtubule. In addition, a single-headed 6-IQ myoVa S1 construct diffuses on microtubules (diffusion coefficient: 0.36 ± 0.13 μm^2/s, $n = 24$; average maximum speed: 5.3 ± 1.2 μm/s, $n = 24$; scan distance: 1.5 ± 0.1 μm, $n = 24$; interaction lifetime: 38 ± 4 s, $n = 47$) as does a full-length myoVa construct having a carboxylated Qdot attached to its cargo-binding domain (data not shown).

MyoVa's association with the microtubule was sensitive to ionic strength, suggesting an electrostatic interaction (Fig. 4*D*). There were a significant number of diffusive events at ionic strengths approaching physiological levels. *In vivo*, it is possible that molecular crowding and the physical nature of the cytoplasm could increase the probability that myoVa interacts with the microtubule. Consistent with this electrostatic mechanism, removing the negatively charged C-terminal "E-hook" from tubulin with subtilisin reduced the number of myoVa molecules diffusing on microtubules by 90% of control (Fig. 4 *D* and *E*) as it does for both kinesin processivity and the diffusional search by MCAK on microtubules (20–22).

These data provide strong evidence that myoVa can undergo a one-dimensional diffusive search along microtubules due to an electrostatic interaction between a domain on the myoVa head and tubulin's E-hook. During its ATPase cycle, the myoVa head interacts weakly with actin through an electrostatic interaction involving a positively charged (+9) surface loop (i.e., loop 2) and the N terminus of actin (23, 24). This same loop may interact with the tubulin E-hook, providing a basis for myoVa's diffusional search along the microtubule surface. In support of this, a single-headed smooth muscle myosin II S1 construct, which also has a positively charged (+5) loop 2, diffuses on microtubules (data not shown). With each head having the capacity to electrostatically interact with the microtubule, myoVa's diffusive search will be enhanced by its double-headed structure as evidenced by longer scanning distances and scan times of two-headed myoVa compared with the single-headed myoVa S1 construct. Even in the absence of cargo, where myoVa exists in a folded/inhibited state, diffusion along the microtubule may still be possible, because inhibition involves the cargo-binding domain interacting with the head while leaving loop 2 fully exposed (11). This diffusive search may provide a mechanism by which the initial encounter between myoVa and kinesin might occur (Fig. 5 *A* and *B*).

Conclusions

A combination of myoVa's hand-over-hand stepping mechanism and inherent flexibility allow the motor to navigate effectively through the overlapping and branched actin filament network in cells (Fig. 5*C*). The ability of myoVa to travel in a spiral fashion along its actin track (25) may also increase its capacity to transfer between polymers in the three-dimensional cytoskeleton. Despite this tendency to switch polymers, myoVa has a high probability of reaching the cell periphery along with any cargo owing to the strong bias in the orientation of actin filaments with the barbed ends toward the plasma membrane (26).

Cargo transport such as melanosomes may involve >60 myoVa, but given the melanosome surface area, only one or two myoVa interact with the actin track (12, 27). Therefore, the present single motor *in vitro* model should reflect the challenges presented by the cytoskeleton *in vivo*. However, myoVa and kinesin do share cargo carrying duties either through their

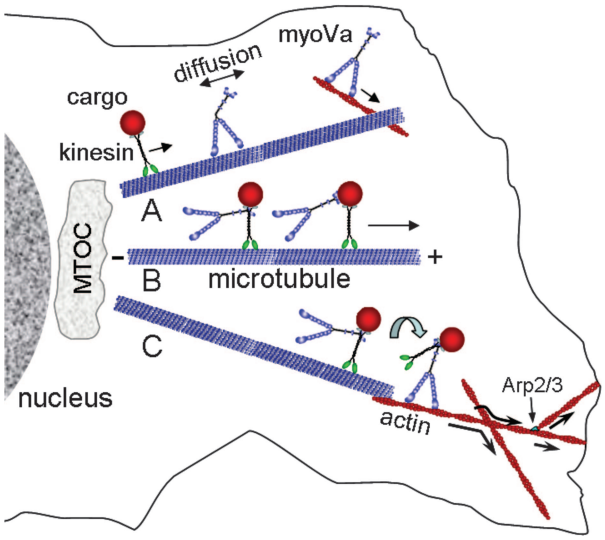

Fig. 5. Illustration of cargo transport model. Organelle transport from the cell center near the nucleus and microtubular organizing center (MTOC) to the cell periphery involves kinesin movement on microtubules with handoff to myoVa for delivery on actin filaments. (*A*) Kinesin, carrying cargo, moves toward the microtubule plus-end (+) and encounters a diffusing myoVa that either landed on or stepped onto the microtubule at a microtubule-actin intersection. The partially bent tail for the diffusing myoVa represents the possibility that myoVa can diffuse in either the extended conformation (see text) or in the folded, inhibited state in the absence of cargo. The processively moving myoVa on actin could be in the extended conformation due to changes in calcium concentration or to cargo-binding. (*B*) Upon encountering myoVa, kinesin and myoVa associate directly through tail–tail interactions or by myoVa binding to the cargo. Kinesin would then continue on toward the periphery. (*C*) Near the periphery, myoVa would then take over cargo delivery on actin tracks. MyoVa can then effectively maneuver through actin intersections and Arp2/3-branched filaments.

individual binding to the same cargo or through direct tail–tail interactions (1, 27, 28) (Fig. 5*B*). The ability of myoVa to undergo a one-dimensional diffusive search along microtubules may allow it to search for a kinesin and/or cargo being transported by a kinesin molecule (Fig. 5*A*). Interestingly, Mooseker and coworkers (29) demonstrated that the tail domain of myoVa can bind microtubules with high affinity, which could provide an additional mechanism for colocalizing myoVa to the microtubular track.

Capturing thermal energy to drive one-dimensional diffusive motion of enzymes and motor molecules along filamentous tracks may be a common strategy to achieve limited motion without active energy consumption (15, 30–33). The capacity of myoVa to interact electrostatically with the microtubule is a new surprise in Mother Nature's toolbox for building complex intracellular systems that contribute not only to determining a cell's phenotype but for coordinating cargo transport by multiple classes of molecular proteins.

Materials and Methods

Protein Preparations. An expressed double-headed heavy meromyoVa with a C-terminal yellow fluorescent protein (13) was modified with an N-terminal biotin tag (6). Streptavidin-functionalized Qdots, emitting at 655 nm (Invitrogen-Molecular Probes, Eugene, OR), were attached to the myoVa by incubating a 1:4 mixture of myoVa and Qdots for 10 min at room temperature in Actin buffer (AB) containing 25 mM KCl, 25 mM imidazole, 1 mM EGTA, 4 mM $MgCl_2$, 10 mM DTT, and oxygen scavengers (0.1 mg/ml glucose oxidase/0.018 mg/ml catalase/2.3 mg/ml glucose), and 1 mg/ml BSA at pH 7.4. Actin was purified from chicken pectoralis as described (34) and prepared as filamentous actin and then labeled with either Alexa Fluor 660 phalloidin or tetramethylrhodamine B isothiocyanate (TRITC) phalloidin. Rhodamine-labeled tubulin and unlabeled tubulin (Cytoskeleton, Denver, CO) were mixed at 1:5 ratio and polymerized as described by the vendor. Microtubules were stabilized with 5 μM taxol. The bovine Arp2/3 complex was purified from bovine thymus (35, 36). Recombinant GST-WASp-VCA was purified from *Escherichia coli* (35, 36).

Motility Assay with Cytoskeletal Intersections and Branches. A 10-μl flow-cell chamber similar to that described (13) was used in generating actin filament intersections *in vitro*. The following solutions were introduced into the flow-cell: (*i*) 0.5 mg/ml *N*-ethyl maleimide (NEM)-modified myosin in myosin buffer (0.3 M KCl/25 mM imidazole/1 mM EGTA/4 mM $MgCl_2$/10 mM DTT, pH 7.4) with a 2-min incubation. The NEM-myosin binds strongly to actin and served to fix the actin to the glass surface. (*ii*) AB wash. (*iii*) AB with 1 mg/ml BSA incubated for 2 min. (*iv*) AB wash. (*v*) 100 nM Alexa Fluor 660 phalloidin-labeled actin filaments in AB, incubated for 2 min. (*vi*) AB wash. (*vii*) 100 nM TRITC-phalloidin labeled actin filaments in AB with 2-min incubation. Because the TRITC-actin was infused last, it served as an intersection to myosin-V by draping over the top of the Alexa Fluor 660 actin. (*viii*) AB wash with desired [ATP]. (*ix*) Qdot-labeled myoVa at 1.25 nM in AB, 1 mg/ml BSA, and desired [ATP].

To create microtubular intersections, all of the steps described above for the actin–actin intersections were repeated except for step *vii*, where fluorescent microtubules (in 1 mM $MgCl_2$/80 mM Pipes, pH 6.9/1 mM EGTA/5 μM taxol) were infused into the flow-cell chamber and allowed to incubate for 2 min.

Branched actin filaments were prepared using Arp2/3 complex. Monomeric actin (500 nM) was polymerized in 50 mM KCl, 10 mM imidazole, 1 mM $MgCl_2$, 1 mM EGTA, 0.2 mM ATP (pH 7.4) at room temperature, resulting in 6- to 10-μm actin filaments in 6 min. We then added 5 nM Arp2/3 complex and 600 nM GST-WASp-VCA followed by an additional 500 nM monomeric actin to generate actin filaments with branches. These filaments were then stabilized by adding 1 μM TRITC-phalloidin. As the branches are very fragile, pipetting was done very gently. Actin filaments with Arp2/3 branches were introduced into the flow-cell at step *v*. After washing with AB and desired [ATP], a mixture of Qdot-labeled myoVa, AB, 1 mg/ml BSA, and 1 mM ATP was infused as described above. All motility assays were performed at 23°C.

MyoVa Movement on Microtubules. Once we observed the movement of Qdot-labeled myoVa on microtubules, a series of experiments and controls were performed in which microtubules were adhered directly to the coverslip surface without any actin present. To observe this movement, microtubules were fixed to the glass surface as described (37). After a 2-min incubation, the flow-cell was washed with AB and then infused with AB with 1 mg/ml BSA. After a 2-min incubation and an AB wash, Qdot-labeled myoVa in AB, 1 mg/ml BSA, and the desired [ATP] (0, 10, 100, 500, 1000 mM) was infused. The experiment was repeated at 25, 50, 75, 100, 125, 150, and 175 mM KCl without ATP. Other control experiments were performed as described.

Subtilisin Digestion of Microtubules. Tubulin (Cytoskeleton, #BK007) at 5 mg/ml in 1 mM GTP, 80 mM Pipes, 1 mM EGTA, 1 mM $MgCl_2$, and 12% glycerol was polymerized at 35°C for 15 min. Taxol was added to 20 μM. To remove the C-terminal ends of α and β- tubulin (E-hook), subtilisin (130 or 325 μg/ml) and microtubules (18 μg/ml) were incubated for 1 h at 35°C. The reaction was stopped by addition of 4 mM PMSF (dissolved in DMSO). The microtubules were pelleted by centrifugation at

14,000 × *g* for 30 min. The supernatant was removed and the pellet resuspended in 80 mM Pipes, 1 mM $MgCl_2$, 1 mM EGTA at room temperature. Samples were analyzed on an 8% acrylamide gel using the Laemmli buffer system. Monoclonal anti-α-Tubulin (cloneB-5-1-2) and anti-β-Tubulin (clone TUB 2.1) antibodies were obtained from Sigma (St. Louis, MO).

Data Acquisition and Image and Data Analysis. Fluorescence imaging was through an objective-type total internal reflectance microscope, as previously described (13), with a software-controlled filter wheel to switch between Qdot and actin/microtubule emission filters. Qdots were excited with the 514-nm argon laser line. Images were obtained by using a DVC-1412:GenIV Intensified high-resolution 12-bit digital camera (DVC Company, Austin, TX) at 83-ms integration time per color and switching between colors every 167 ms. Images were processed by using QED In Vivo software (Media Cybernetics, Silver Spring, MD).

Typically, 300 images per color were recorded for a total of 100 s. Digital images were corrected for image registration error between colors. The position of Qdot-labeled myoVa was fitted to a two-dimensional Gaussian representing the Qdot point-spread function with 6-nm accuracy (6, 8). As a Qdot-labeled myoVa approached an intersection, the absolute position of the Qdot to the center of the intersecting actin filament or microtubule was determined as follows. Using Image J 1.34s (National Institutes of Health, Bethesda, MD), the 100-s movie file was split into two TIFF stacks (300 frames each), red for the Qdot and green for the actin/microtubule. Because the filaments were fixed to the surface, the filament images were averaged over all 300 frames. Then five scan lines were drawn (separated by 1 pixel = 55 nm) that passed through the Qdot and the actin filament at a perpendicular angle using both the red and green TIFF stacks (see SI Fig. 7). The intensity along each scan line was exported to Sigma Plot and then averaged. The resultant average intensity scan through the Qdot and the filament were each fitted to a Gaussian, with the distance between Gaussian peaks defined as the distance between center of actin filament and Qdot. Accuracy of the distance measurement was 6 nm.

To measure the intersection angle between the Alexa Fluor 660- and TRITC-actin filaments, the 100-s movie file was once again split into two TIFF stacks. Then, all of the images within each stack were added to generate a new composite image for each color. This operation resulted in a linear track associated with the moving Qdot-labeled myoVa (red stack) and a bright TRITC-actin filament (green stack). The intersection angle was then determined by lines drawn visually along the myoVa trajectory as it approached the intersection and the TRITC-actin filament.

For myoVa diffusing on microtubules, the maximum speed of diffusion for a given encounter was defined as the maximum displacement along the microtubule during one image frame multiplied by the frame rate (i.e., three frames per s). The scan distance was measured as the distance between the two extreme positions the myoVa achieved during its one-dimensional diffusive encounter, whereas the interaction time was the total time between the initial appearance of the myoVa on the microtubule and its disappearance, presumably due to the myoVa diffusing away from the microtubule.

We thank Neil Kad, Ned Debold, Hailong Lu, and Kazuhiko Kinosita, Jr., for critical discussions; Samantha Beck for superb technical assistance; and Richard Cheney and Mark Mooseker for their helpful critiques of our manuscript. This work was supported by National Institutes of Health Grants AR47906 (to D.M.W.), HL38113 (to K.M.T.), GM026338 (to T.D.P.), and GM072123 (to R.M.).

1. Huang JD, Brady ST, Richards BW, Stenoien D, Resau, JH, Copeland NG, Jenkins NA (1999) *Nature* 397:267–270.
2. Langford GM (2003) *Traffic* 3:859–865.
3. Brown JR, Stafford P, Langford GM (2004) *J Neurobiol* 58:175–188.
4. Brown SS (1999) *Annu Rev Cell Dev Biol* 15:63–80.
5. Mehta AD, Rock RS, Rief M, Spudich JA, Mooseker MS, Cheney RE (1999) *Nature* 400:590–593.
6. Warshaw DM, Kennedy GG, Work SS, Krementsova EB, Beck S, Trybus KM (2005) *Biophys J* 88:L30–L32.
7. Sellers JR, Veigel C (2006) *Curr Opin Cell Biol* 18:68–73.
8. Yildiz A, Forkey JN, McKinney SA, Ha T, Goldman YE, Selvin PR (2003) *Science* 300:2061–2065.
9. Churchman LS, Okten Z, Rock RS, Dawson JF, Spudich JA. (2005) *Proc Natl Acad Sci USA* 102:1419–1423.
10. Syed S, Snyder GE, Franzini-Armstrong C, Selvin PR, Goldman YE (2006) *EMBO J* 25:1795–1803.
11. Liu J, Taylor DW, Krementsova EB, Trybus KM, Taylor KA (2006) *Nature* 442:208–211.
12. Snider J, Lin F, Zahedi N, Rodionov V, Yu CC, Gross SP (2004) *Proc Natl Acad Sci USA* 101:13204–13209.
13. Baker JE, Krementsova EB, Kennedy GG, Armstrong A, Trybus KM, Warshaw DM (2004) *Proc Natl Acad Sci USA* 101:5542–5546.
14. Rosenfeld SS, Sweeney HL (2004) *J Biol Chem* 279:401000–401011.
15. Walker ML, Burgess SA, Sellers JR, Wang F, Hammer JA, III, Trinick J, Knight PJ (2000) *Nature* 405:804–807.
16. Purcell TJ, Sweeney HL, Spudich JA (2005) *Proc Natl Acad Sci USA* 102:13873–13878.
17. Amann JK, Pollard TD (2001) *Proc Natl Acad Sci USA* 98:15009–15013.
18. Volkmann N, Amann KJ, Stoilova-Mcphie S, Egile C, Winter DC, Hazelwood L, Heuser JE, Li R, Pollard TD, Hanein D (2001) *Science* 293:2456–2459.
19. Howard J (2001) in *Mechanics of Motor Proteins and the Cytoskeleton* (Sinauer, Sunderland, MA), pp 49–73.
20. Helenius J, Brouhard G, Kalaidzidis Y, Diez S, Howard J (2006) *Nature* 441:115–119.
21. Okada Y, Hirokawa N (2000) *Proc Natl Acad Sci USA* 97:640–645.
22. Lakamper S, Meyhofer E (2005) *Biophys J* 89:3223–3234.
23. Yengo CM, Sweeney HL (2004) *Biochemistry* 43:2605–2612.
24. Volkmann N, Liu H, Hazelwood L, Krementsova EB, Lowey S, Trybus KM, Hanein D (2005) *Mol Cell* 19:595–605.
25. Ali MY, Uemura S, Adachi K, Itoh H, Kinosita K, Jr, Ishiwata S (2002) *Nat Struct Biol* 9:464–467.
26. Svitkina TM, Bulanova EA, Chaga OY, Vignjevic DM, Kojima S, Vasiliev JM, Borisy GG (2003) *J Cell Biol* 160:409–421.
27. Gross SP, Tuma MC, Deacon SW, Serpinskaya AS, Reilein AR, Gelfand VI (2002) *J Cell Biol* 156:855–865.
28. Rogers SL, Gelfand VI (2000) *Curr Opin Cell Biol* 12:57–62.
29. Cao TT, Chang W, Masters SE, Mooseker MS (2004) *Mol Biol Cell* 15:151–161.
30. Blainey PC, van Oijen AM, Banerjee A, Verdine GL, Xie XS (2006) *Proc Natl Acad Sci USA* 103:5752–5757.
31. Wang Z, Sheetz MP (1999) *Cell Struct Funct* 24:373–383.
32. Culver-Hanlon TL, Lex SA, Stephens, Quintyne NJ, King SJ (2006) *Nat Cell Biol* 8:264–270.
33. Kobayashi T, Shiroguchi K, Edamatsu M, Toyoshima YY (2006) *Biochem Biophys Res Commun* 340:23–28.
34. Pardee JD, Spudich JA (1982) *Methods Cell Biol* 24:271–289.
35. Higgs HN, Blanchoin L, Pollard TD (1999) *Biochemistry* 38:15212–15222.
36. Hufner K, Higgs HN, Pollard TD, Jacobi C, Aepfelbacher M, Linder S (2001) *J Biol Chem* 276:35761–35767.
37. Kawaguchi K, Ishiwata S (2000) *Biochem Biophys Res Commun* 272:895–899.